ACS Catalysis

Research Article

pubs.acs.org/acscatalysis

Universality in Oxygen Reduction Electrocatalysis on Metal Surfaces

Venkatasubramanian Viswanathan,[†] Heine Anton Hansen,[‡] Jan Rossmeisl,[§] and Jens K. Nørskov*[,‡,⊥]

[†]Department of Mechanical Engineering and [‡]Department of Chemical Engineering, Stanford University, Stanford, California, 94305-3030, United States

[§]Center for Atomic-scale Materials Design, Department of Physics, Technical University of Denmark, DK-2800, Lyngby, Denmark

[⊥]SUNCAT, SLAC National Accelerator Laboratory, Menlo Park, California 94025-7015, United States

Supporting Information

ABSTRACT: In this work, we extend the activity volcano for oxygen reduction from the face-centered cubic (fcc) metal (111) facet to the (100) facet. Using density functional theory calculations, we show that the recent findings of constant scaling between OOH* and OH* holds on the fcc metal (100) facet, as well. Using this fact, we show the existence of a universal activity volcano to describe oxygen reduction electrocatalysis with a minimum overpotential, η_{min} = 0.37 ± 0.1 V. Specifically, we find that the (100) facet of Pt is found to bind oxygen intermediates too strongly and is not active for oxygen reduction reaction (ORR). In contrast, Au(100) is predicted to be more active than Au(111) and comparable in activity to Pt alloys. Using this activity volcano, we further predict that Au alloys that bind OH more strongly could display improved ORR activity on the (100) facet. We carry out a computational search over candidate alloys and suggest that alloying Au with early transition metals could lead to materials that exhibit enhanced ORR activity. We also prescribe a simple principle in the choice of nanoparticle catalysts in which the chosen catalyst should have its dense facet on the weak binding leg of the volcano so that its more open facets and defects could also be active.

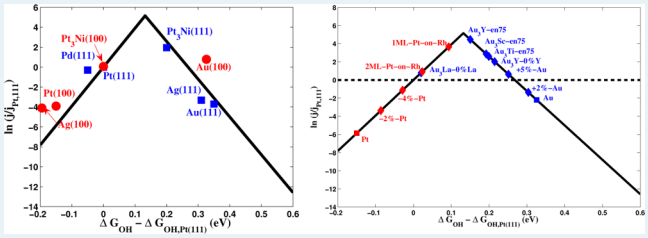

KEYWORDS: *activity volcano, oxygen reduction, nanoparticles, fuel cells, electrocatalysis*

1. INTRODUCTION

Low operating temperatures, quiet operation, and high theoretical efficiencies, among a host of other features, make polymer electrolyte membrane fuel cells (PEM-FCs) an attractive energy conversion device, especially for portable electronics devices and applications in transportation. However, the sluggish electrochemical kinetics of the oxygen reduction reaction (ORR) occurring at the cathode typically catalyzed by nanometer sized platinum particles limit the performance of these cells.

Using a simple model, Nørskov et al.[1] argued that the ideal catalyst for the oxygen reduction reaction needs to activate molecular oxygen while, at the same time, binding oxygen species such as O, OH weakly. Using density functional theory (DFT) calculations on model fcc (111) surfaces, a simple model was able to successfully predict trends in the activity of metal catalysts for ORR.[1] The validity of this model for the (111) facets was further illustrated by a computational screening study performed by Greeley et al.,[2] in which they identified a new class of catalysts using this model that were subsequently found to be experimentally more active than Pt. However, the state-of-the-art Pt nanoparticles typically contain both hexagonal (111) facets and square (100) facets. To optimize the activity of these nanoparticle catalysts, it is important to consider the activity of the (100) facets, as well. This was the focus of an earlier study by Greeley et al.,[3] in which an activity volcano for the (100) facet was constructed. This was done over a broad range of metals, and the overall trend in activity between the different metals was well-described. In this work, we extend this analysis to construct a more accurate description of the top of the volcano by using a more appropriate descriptor. This reconciles the discrepancies between the predictions of the earlier model for the most active materials and experiments. We also show that the recent findings of constant scaling between OOH* and OH* holds for the fcc metal (100) facet, as well. This leads to the existence of a universal activity volcano to describe oxygen reduction electrocatalysis. We also build simple design principles for nanoparticle catalysts and provide interesting candidate materials that could be highly active for oxygen reduction reaction.

2. RESULTS AND DISCUSSION

2.1. Free Energy Diagram. We follow the associative mechanism for the oxygen reduction reaction on fcc metal (111) facets as outlined in earlier works:[1,4]

$$O_2(g) + 4H^+ + 4e^- + * \rightarrow OOH^* + 3H^+ + 3e^- \quad (1a)$$

$$OOH^* + 3H^+ + 3e^- \rightarrow O^* + H_2O(l) + 2H^+ + 2e^- \quad (1b)$$

Received: April 5, 2012
Revised: June 18, 2012
Published: June 19, 2012

   dx.doi.org/10.1021/cs300227s | ACS Catal. 2012, 2, 1654−1660

$$O^* + H_2O(l) + 2H^+ + 2e^- \rightarrow OH^* + H_2O(l) + H^+ + e^- \quad (1c)$$

$$OH^* + H_2O(l) + H^+ + e^- \rightarrow * + 2H_2O(l) \quad (1d)$$

The mechanism involves a sequential addition of a proton and electron in each elementary step. In this analysis, we have excluded the two-electron reduction to H_2O_2. This assumption is made because no ring current associated with the production of H_2O_2 is detected on Pt and Pt alloys at these potentials.[5]

The free energies of different intermediates involved in the mechanism are calculated at standard conditions and a potential of $U = 0$ V versus the reversible hydrogen electrode using the relation

$$\Delta G^0 = \Delta E_{w,water} + \Delta ZPE - T\Delta S \quad (2)$$

where $\Delta E_{w,water}$ is the formation energy of an intermediate, including the stabilization of water, calculated relative to H_2O and H_2; ΔZPE is the difference in zero point energies, and ΔS is the change in entropy. The reference O_2 energy is obtained from fitting to the experimental reaction energy for H_2O formation to avoid the well-known errors made by DFT in describing O_2. This is similar to that used in earlier works, and we use the zero point energies and entropic corrections as reported previously.[1,4] A potential of $U = 0$ V versus the reversible hydrogen electrode implies the relation $\Delta G_{H^+} + \Delta G_{e^-} = 1/2\Delta G_{H_2(g)}$. This relation provides a way to computationally calculate the sum of the free energy of proton and electron and is termed as the computational hydrogen electrode.[1] The effect of a potential, U, is included by shifting the free energy of an electron by $-eU$, and the free energy at a potential U can thus be calculated using the relation $\Delta G = \Delta G^0 - eU$, where U is the potential relative to the reversible hydrogen electrode. This procedure can be used to construct the free energy diagrams and can be used to deduce an important parameter, the potential-determining step, which is defined as the last step that becomes downhill in free energy when the overpotential is increased.[1]

In the case of materials that bind oxygen intermediates too strongly, it has been found that reaction 1d is the potential-determining step.[4] Therefore, the free energy difference of the limiting step is given by

$$\Delta G_{r4} = \Delta G_{H_2O(l)} - \Delta G_{OH^*} \quad (3)$$

In the case of the materials that bind oxygen intermediates too weakly, it has been found that reaction 1a is the potential-determining step.[4] Therefore, the free energy difference of the limiting step is given by

$$\Delta G_{rl} = \Delta G_{OOH^*} - \Delta G_{O_2(g)} \quad (4)$$

Therefore, the current density for the materials on the left and right leg of the volcano are given by

$$j_L = j_0 \exp\left[\frac{-\Delta G_{r4}}{kT}\right] \quad (5a)$$

$$j_R = j_0 \exp\left[\frac{-\Delta G_{rl}}{kT}\right] \quad (5b)$$

Here, we have assumed Tafel kinetics with a charge transfer coefficient of 1, implying that only thermodynamic limitations determine the overpotential. In addition, we also assume that the electrochemical prefactors for the two different limiting reactions for the left and the right legs of the volcano are the same.[6] Although a difference in the prefactors could alter the exact location of the top of the activity volcano, an order of magnitude difference in prefactors results in a shift of only 60 meV, and thus, we would expect the conclusions in trends to be reasonably accurate.

2.2. Scaling Relations. As shown in the earlier section, the position of the two legs of the volcano are governed by the stability of OH* and OOH*, respectively. Recently, it has been shown that the free energy difference between OH* and OOH* is almost constant, independent of the binding strength to the surface for oxide surfaces.[7] This observation was made by Koper,[8] who noted that the binding strength of OH* and OOH* are related to each other by a constant amount of ≈3.2 eV for metal (111) facets and oxide surfaces, regardless of the binding site. The slope of unity between the binding energies of OH* and OOH* reflects the fact that both species have a single bond between an O atom and the metal surface. The constant intercept is a consequence of similar binding sites of OH* and OOH*. It is interesting to note that this constant scaling even holds in aqueous solutions and implies that there is a universal scaling relation between OH* and OOH*. Here, we explore this scaling relation for materials on the (100) facet and find that it holds for the (100) facet, as shown in Figure 1. The best linear fit obtained

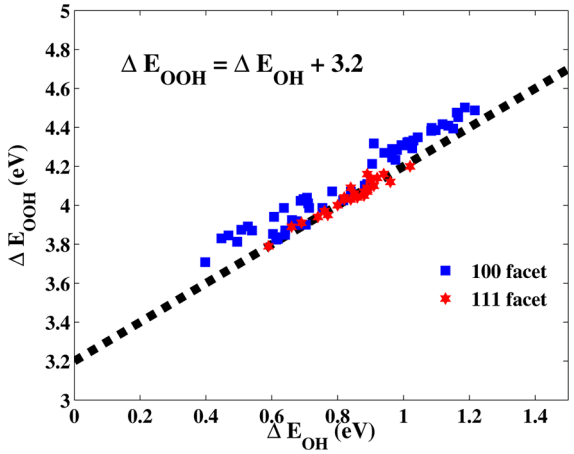

Figure 1. Binding energy of OOH* plotted against the adsorption energy of OH* on fcc (111) and (100) facets. The binding energies do not include zero point energy and entropy corrections. The calculated stabilization due to the water layer has been included for the (111) facet, and this corresponds to 0.3 and 0.5 eV stabilization for OOH* and OH*, respectively. The constant scaling line of $\Delta E_{OOH^*} = \Delta E_{OH^*} + 3.2$ is also shown for comparison, and 95% of the points are within ±0.2 eV.

for the (100) facet is $\Delta E_{OOH^*} = \Delta E_{OH^*} + 3.29$, which is within 0.1 eV of the 3.2 eV constant scaling reported in earlier work. This scaling relation does not include additional stabilization due to the water layer, which is expected to be small on the (100) facet.

The constant difference between the adsorption free energies of OH* and OOH* of 3.2 eV sets a limit on the minimum thermodynamic overpotential for ORR on metal surfaces. The optimal catalyst is one in which there is an equal splitting of the remaining available potential for the activation of OOH* and reduction of OH*. The overall change in free energy associated with the four-electron reduction of O_2 to H_2O is given by the Nernst equation, $\Delta G^0 = -4E^0$. Using the equilibrium potential of $E^0 = 1.23$ V, we get an overall free energy change of $\Delta G^0 = -4 \times 1.23 = -4.92$ eV. However, because of the constant scaling between OH* and OOH*, the available free energy for the two

dx.doi.org/10.1021/cs300227s | ACS Catal. 2012, 2, 1654−1660

remaining electrochemical reactions involved is given by ΔG_{ava} = −4.92 + 3.2= −1.72 eV. The limiting potential on the optimal catalyst is given by $U_{min} = -\Delta G_{ava}/2e$ = 0.86 V. The scaling relation between OH* and OOH* has a scatter of ∼0.2 eV, and thus, this sets the minimum thermodynamic overpotential of η_{min} = 1.23 − 0.86 ± 0.1 = 0.37 ± 0.1 V for ORR, regardless of the metal facet considered.

2.3. Activity Volcano. Here, we derive explicitly the activity volcano for the (111) and (100) facets and show that they can be described by a single universal volcano.

2.3.1. (111) Facets. To make the comparison more evident, we normalize all the current density relative to Pt(111), as has been done in earlier work.[2] Because Pt(111) is on the strong OH-binding leg, the limiting step is the reduction of OH* to H_2O. Thus, the activity for the materials on the strong OH-binding leg of the (111) volcano normalized to Pt(111) is given by

$$kT \ln\left(\frac{j}{j_{Pt111}}\right) = (\Delta G_{r4,Pt111} - \Delta G_{r4,X111}) = \left(\Delta G_{OH,X111} - \Delta G_{OH,pt111}\right) = (\Delta E_{OH,X111} - \Delta E_{OH,Pt111}) \quad (6)$$

Here, we have made the assumption that the zero-point energy and entropic corrections are constant between the materials under consideration and similar to that used earlier.[2]

The activity of materials on the right leg of the (111) volcano is given by

$$\begin{aligned} kT \ln\left(\frac{j}{j_{Pt111}}\right) &= (\Delta G_{r4,Pt111} - \Delta G_{r1,X111}) \\ &= \left(\Delta G_{H_2O(l)} - \Delta G_{OH,Pt111}\right) - \left(\Delta G_{OOH,X111} - \Delta G_{O_2(g)}\right) \\ &= \left(\Delta G_{H_2O(l)} - \Delta G_{OH,Pt111}\right) - (\Delta G_{OOH,X111} - \Delta G_{OOH,Pt111}) - \left(\Delta G_{OOH,Pt111} - \Delta G_{O_2(g)}\right) \\ &= 0.26[\text{eV}] - (\Delta G_{OOH,X111} - \Delta G_{OOH,Pt111}) \\ &= 0.26[\text{eV}] - (\Delta E_{OOH,X111} - \Delta E_{OOH,Pt111}) \\ &= 0.26[\text{eV}] - \alpha(\Delta E_{OH,X111} - \Delta E_{OH,Pt111}) \end{aligned} \quad (7)$$

The value of $(\Delta G_{r4,Pt111} - \Delta G_{r1,Pt111})$ is $(\Delta G_{H_2O(l)} - \Delta G_{OH,Pt111}) - (\Delta G_{OOH,Pt111} - \Delta G_{O_2(g)})$ = 0.26 eV, which is taken from the potential energy diagram of Pt(111).[2] We again make the simplifying assumption that zero point energies and entropic corrections for OOH* are constant between materials, and thus, the free energy difference is given by the binding energy difference, $(\Delta G_{OOH,X111} - \Delta G_{OOH,Pt111}) = (\Delta E_{OOH,X111} - \Delta E_{OOH,Pt111})$. Using the correlation of binding energies for materials close to the top of the volcano, we show that $(\Delta E_{OOH,X111} - \Delta E_{OOH,Pt111}) = \alpha(\Delta E_{OH,X111} - \Delta E_{OH,Pt111})$, with α = 0.97. The binding energies of OH* and OOH* are listed in the Supporting Information. It is to be noted that in this work, we plot the oxygen reduction activity in terms of the OH binding energy, but in earlier works, this has been plotted in terms of the O binding energy. Although the binding energy of O and OH scale with each other,[9] the choice of OH is made in this work because it is easier to determine the average strength of OH binding experimentally by the position of the oxidative peak in a cyclic voltammogram in a N_2 environment.[10,11] This choice is more appropriate because it directly determines the activity for materials on the left leg of the volcano. A similar choice has been made in a recent work, and the position of the OH peak obtained from cyclic voltammograms has been used directly to correlate with the oxygen reduction activity.[10]

2.3.2. (100) Facets. We follow the same mechanism as that on the (111) facet. Although there might be other pathways, such as O_2 dissociation, that might be possible on the more open (100) facet, we believe that these likely will not affect the materials near the top of the volcano. The O_2 dissociation pathway is expected to be active only on materials that bind O* strongly, and these materials are expected to bind OH* strongly, as well, and these materials would lie on the strong binding leg of the volcano. We follow an approach similar to that in the previous section, and the activity of materials on the left leg of the (100) volcano is given by

$$\begin{aligned} kT \ln\left(\frac{j}{j_{Pt111}}\right) &= (\Delta G_{r4,Pt111} - \Delta G_{r4,X100}) \\ &= (\Delta G_{OH,X100} - \Delta G_{OH,Pt100}) + (\Delta G_{OH,Pt100} - \Delta G_{OH,Pt111}) \\ &= (\Delta E_{OH,X100} - \Delta E_{OH,Pt100}) + (\Delta G_{OH,Pt100} - \Delta G_{OH,Pt111}) \\ &= (\Delta E_{OH,X100} - \Delta E_{OH,Pt100}) - 0.15[\text{eV}] \end{aligned} \quad (8)$$

Here, we note that the stabilization of OH* in the water layer for (111) and (100) facets is expected to be different.[3] This is due to the lack of registry of the square symmetry of the (100) surface with the hexagonal H_2O−OH overlayer. We estimate a value of $(\Delta G_{OH,Pt100} - \Delta G_{OH,Pt111})$ = −0.15 eV from the relative shifts of the first oxidative OH peak from the cyclic voltammogram. This corresponds to a water stabilization of about 0.1 eV for OH* on the (100) facet, and this is significantly lower than the 0.5 eV

dx.doi.org/10.1021/cs300227s | ACS Catal. 2012, 2, 1654−1660

stabilization of OH* on the (111) facet. The assignment of the first oxidative peak for Pt(111) is around 0.7 V;[12] for Pt(100), it is around 0.55 V.[13] This assignment is also consistent with recent first-principles simulations.[14] The location of these peaks directly corresponds to the free energy of OH* formation,[11] and a difference of the potentials for the oxidative peak directly gives the free energy difference of OH* on the two metal facets. The assignment of the first oxidative peak to OH* for (111) and (100) is also consistent with the calculated stability of O* and OH* on the (100) facet.

The activity of materials on the weak OH-binding leg of the (100) volcano is given by

$$
\begin{aligned}
kT\ln\left(\frac{j}{j_{\mathrm{Pt111}}}\right) &= (\Delta G_{\mathrm{r4,Pt111}} - \Delta G_{\mathrm{r1,X100}}) \\
&= \left(\Delta G_{\mathrm{H_2O(1)}} - \Delta G_{\mathrm{OH,Pt111}}\right) - \left(\Delta G_{\mathrm{OOH,X100}} - \Delta G_{\mathrm{O_2(g)}}\right) \\
&= \left(\Delta G_{\mathrm{H_2O(1)}} - \Delta G_{\mathrm{OH,Pt111}}\right) - \left(\Delta G_{\mathrm{OOH,X100}} - \Delta G_{\mathrm{O_2(g)}}\right) \\
&= \left(\Delta G_{\mathrm{H_2O(1)}} - \Delta G_{\mathrm{OH,Pt111}}\right) - (\Delta G_{\mathrm{OOH,X100}} - \Delta G_{\mathrm{OOH,Pt100}}), \\
&\quad -(\Delta G_{\mathrm{OOH,Pt100}} - \Delta G_{\mathrm{OOH,Pt111}}) - \left(\Delta G_{\mathrm{OOH,Pt111}} - \Delta G_{\mathrm{O_2(g)}}\right) \\
&= 0.26[\mathrm{eV}] + 0.15[\mathrm{eV}] - \alpha(\Delta E_{\mathrm{OH,X100}} - \Delta E_{\mathrm{OH,Pt100}}) \qquad (9)
\end{aligned}
$$

We assume $(\Delta G_{\mathrm{OOH,Pt100}} - \Delta G_{\mathrm{OOH,Pt111}}) \approx (\Delta G_{\mathrm{OH,Pt100}} - \Delta G_{\mathrm{OH,Pt111}}) = -0.15$ eV as a result of the observations made earlier regarding the constant scaling between OOH* and OH*. The value chosen is close to the difference in the binding energy on the two facets, $\Delta E_{\mathrm{OOH,Pt100}} = 3.87$ eV and $\Delta E_{\mathrm{OOH,Pt111}} = 4.06$ eV.[3,4] Using the correlation of binding energies for materials close to the top of the volcano, $\alpha = 0.97$ is obtained for the (100) facet as well. The binding energies of OH* and OOH* are listed in the Supporting Information.

The fcc (111) metal facets can be positioned on the activity volcano directly by the binding energy relative to Pt(111), and this is shown in Figure 2; however, for the metals on the (100) facet, the location on the activity volcano is given by calculating a binding energy relative to Pt(100) and positioning it with a shift of −0.15 eV. This shift accounts for the differences in free energy corrections between Pt(111) and Pt(100) and a single universal volcano describes the activity on both the (111) and (100) facets, which is shown in Figure 2.

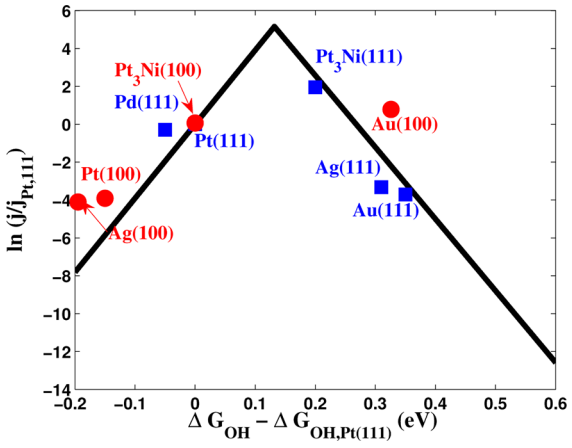

Figure 2. Universal activity volcano for ORR showing the experimental current density as a function of the calculated free energy of OH. The experimental data are taken from Wang et al.[12] for Pt(111), Shao et al.[20] for Pd(111), Blizanac et al.[21] for Ag(111) and Ag(100), Stamenkovic et al.[5] for $Pt_3Ni(111)$ and $Pt_3Ni(100)$, Blizanac et al.[17] for Au(100), and Schmidt et al.[19] for Au(111).

2.4. Surface Structure. We address the issue of the hex-reconstruction before making comparisons of the results of the model to experiments. It is to be noted that (100) surfaces when prepared in UHV by sputtering and annealing typically reconstruct into a hexagonal-densely packed form.[15] However, recent STM imaging of the Pt(100) surface shows that in contact with electrolytes, the Pt(100)-hex surface, prepared either in UHV or by a flame annealing method, is lifted and becomes a (1 × 1) surface with many defects.[16] The defect sites are expected to bind O intermediates strongly and, thus, are likely inactive; we would expect the activity to be dominated by the Pt(100)-(1 × 1) surface sites. This is also true of the Au(100) facet, where the potential induced "hex" → (1 × 1) transition occurs in the cathodic potential range.[17] This gives us confidence in making comparisons of the results of our model to the rotating disk electrode (RDE) experiments. In addition, the focus of this work is to aid the design of nanoparticle catalysts where we would not expect the reconstruction of the (100) facets.[3]

2.5. Comparison to Experiments. We have made a comparison of our model for the activity to several rotating disk electrode (RDE) experiments on well-defined surfaces and this is shown in Figure 2. The experimental measurements in acidic environment considered for comparison are all carried out in 0.1 M $HClO_4$. The experimental measurement of Au(100) in an alkaline environment is carried out in 0.1 M KOH. All experiments are carried out at a rotation speed of 1600 rpm. The choice of $HClO_4$ was made because it is a nonadsorbing electrolyte and does not compete with the oxygen intermediates for adsorption.[18] We have intentionally avoided H_2SO_4 because bisulphate ions are known to adsorb strongly on fcc metal (111) surfaces, and this could significantly affect the binding energy of oxygen intermediates. The relative shifts in the half-wave potential are used to plot the experimental activity. This was chosen so that we could include a wide range of materials with a drastically varying OH binding energy. Here, to make a direct comparison with the predictions from our model, we have assumed that the Tafel slopes for the oxygen reduction reaction is the same for these materials. However, this assumption does not affect the conclusions made about the trends in activity of the different materials considered.

dx.doi.org/10.1021/cs300227s | ACS Catal. 2012, 2, 1654−1660

From Figure 2, it can be seen that there is a good agreement between the predicted activity for different materials on the (100) facet. A general trend that is observed is the expected stronger binding of OH-binding intermediates on (100), which makes the (100) surface lie to the left of the corresponding (111) facet. As a result, the metals, whose (111) facets lie on the strong OH-binding leg, have lower activity on their (100) facets. As a result, the materials of interest for the (100) facet are the materials on the weak OH-binding leg of the (111) facet. We note that among these, Au(100) looks the most promising lying on the weak binding side of the volcano. Here, we have included only the experimental measurement of ORR on Au(100) in alkaline environment. We note that on Au(111), there is ring current observed, suggesting that the product is H_2O_2, but this is not observed in the case of Au(100).[17,19] This difference could be due to the extremely weak binding of OOH* on Au(111), thereby making addition of the next proton facile and leading to the production of H_2O_2. However, a more detailed analysis is required to address the issue of selectivity of the production of H_2O_2 and H_2O. The other metals, such as Pt, Pd, and Ag, lie on the stronger binding leg of the volcano and are found to be inactive. In this analysis, we have limited the comparison of our model to nonadsorbing electrolyte $HClO_4$. These trends are more complicated in adsorbing electrolytes, such as H_2SO_4, where the adsorption of bisulphate ion also needs to be considered. We have also neglected the effect of the electric field on the adsorption energies of the oxygen intermediates on (100) surfaces; however, these effects have been typically found to be small on (111) surfaces, and we would expect a similar trend on the (100) surfaces.[4]

In the search for candidate materials with active (100) facets, two possibilities exist: (a) a compression of Pt and (b) an expansion of Au. We have pursued both of these avenues in the search for alloy catalysts that could be highly active for oxygen reduction reaction.

2.6. Screening Candidate Alloys. The universal activity volcano shows that it is possible to find materials whose (100) facets are as active as the most active (111) materials. This could be achieved, for example, by weakening the binding of OH by about 0.3 eV from that on Pt(100) or by strengthening the binding of OH by 0.2 eV from that on Au(100).

To assess the possible enhanced activity of modified Pt surfaces, we have calculated the binding energy of OH* on compressed Pt(100), Pt monolayers on Rh(100), and Pt skins on some Pt_3X alloys suitably chosen based on the screening study by Greeley et al.[2] The solute elements chosen for the Pt_3X alloys are X = {Y, Sc, V, Ta, Ni, Nb}. The Pt_3X alloys are modeled in the L_{12} structure, so alternating surface layers in the (100) direction have 100% Pt in one layer followed by 50% Pt and 50% of the solute element X in the next layer. Depending on preparation and possibly dissolution of the solute atoms in the electrochemical environment, Pt_3X alloys may have varying degrees of solute in the subsurface.[10] We have modeled surfaces with a Pt skin in the top layer and either 75%, 50%, or 0% X in the second layer, where the surface with 50% X in the second layer corresponds to a stoichiometric Pt_3X surface. Subsurface X content higher than 50% may be reached by vacuum annealing, leading to the formation of a Pt skin.[5]

We find that pure compression of Pt(100) up to 4% is not sufficient to weaken the OH binding to reach the top of the volcano, as seen in Figure 3. One interesting candidate that weakens the OH binding further is a Pt monolayer on Rh(100). This weakening cannot be explained by the effect of strain alone because Rh causes only a 4% compression relative to Pt. For all the Pt_3X alloys considered, it is found that increasing the solute concentration in the second layer decreases OH binding, and the weakest OH binding is obtained with 0% Pt in the second layer. The $Pt_3Ni(100)$ surfaces with 75% X in the subsurface has an OH binding energy 0.16 eV weaker than on Pt(100). The resulting activity predicted by our volcano is in good agreement with experiments on the vacuum-annealed surface by Stamenkovic et al.[5] and this is shown in Figure 2.

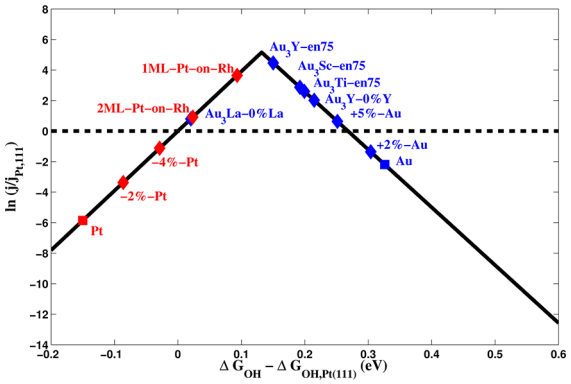

Figure 3. ORR activity volcano on the fcc (100) facet with interesting candidate materials. Pt and Au are shown in red and blue ■, respectively, and modified Pt and Au candidates are shown in red and blue ◆, respectively. +x% corresponds to an expansion of x% from that of bulk Au, and −x% corresponds to a compression of x% from that of bulk Pt. For the Au_3X alloys, the y%X refers the solute concentration in the second layer.

To assess the activity of modified Au(100) surfaces, we have calculated the OH binding energy on expanded Au(100) and Au skins in Au_3X alloys in the L_{12} structure, shown in Figure 3. For the Au_3X alloys, the solute elements considered are X = {In, Y, Zr, Sc, Pd, La, Hf, Al, Ti}. There is only 0.05 eV stabilization of OH on Au(100) by 4% expansion of the lattice. Thus, expansion alone is unlikely to lead to significant improvements in activity. For the Au_3X alloys, we find that alloys enriched with 75% X in the second layer for early transition metals such as Sc, Ti, and Y have nearly optimal strengthening of the OH binding energy. Although it is possible that these enriched alloys might not be stable in electrochemical environments, we find that no Y or La in the second layer still strengthens the OH binding energy by a significant amount. In the case of Au_3La, the alloy is expanded by 8% relative to Au, and it binds OH much too strongly. It is possible a thicker Au skin or a facet of a more gold rich Au−La alloy such as Au_6La would bind OH more weakly and be more active than Au_3La. Au_3Y and Au_3Sc lie quite close to the top of the volcano but still lie on the weak binding side. These alloys are 5% expanded relative to pure Au, so the effect of having Y in the fourth layer from the surface is a slight stabilization of OH* by 0.04 eV, moving it closer to the top of the volcano. It is to be noted that these alloys might not be stable in electrochemical environments. However, it is worth pointing out that the strategy of alloying Au with early transition metals could be advantageous. This is due to a cooperative effect of lattice expansion and ligand effect. We could expect improved activity over a wide range of solute concentrations, as has been observed in the case of Pt alloys.[22]

2.7. Implication for Nanoparticle Catalysts. A well-faceted nanoparticle typically consists of (111) and (100) facets, along with edges and corner sites. In a recent study, Kleis et al. showed that for particle sizes larger than 3 nm, the binding

energy on the microfacets of these particles converge to the values on the extended (111) and (100) facets.[23] It has also been shown that the effects of edges and corners are local, and these do not significantly affect the binding energy of intermediates beyond their nearest row of atoms.[24] These observations lend credence to the applicability of our model based on extended surfaces to predict trends in nanoparticle activity.

Recent advancements following the pioneering work of El-Sayed et al.[25] have made the shape-controlled synthesis of different nanostructured morphologies possible using different Pt precursors, capping agents, reducing agents, and solvents. A more detailed discussion of the synthetic approaches to form different morphologies can be found in a recent review by Feliu et al.[26] A recent study on the structure-sensitive catalysis on different shape-controlled Pt nanoparticles showed the following trend: $PtNP_{hexahedral} > PtNP_{tetrahedral} \approx PtNP_{spherical} > PtNP_{cubic}$ in 0.1 M $HClO_4$.[27] This has been attributed to the preferential (111) surface facets present in $PtNP_{tetrahedral}$ and (100) facets present in $PtNP_{cubic}$, which results in a noticeable switch in activity for ORR. This trend is consistent with our model and also lends further support to the applicability of extended surfaces to describe nanofaceted catalysts.

In the case of gold, the most active nanoparticle is expected to be the one in which the number of (100) sites is maximized. However, Au surfaces are well-known to reconstruct, as discussed earlier,[15] and thus, conclusive assignment of the presence of different facets under electrochemical conditions is necessary to correlate its electrocatalytic activity. Lead underpotential deposition (UPD) has been used to conclusively point out the presence of different kinds of surface sites on gold nanoparticles.[28,29] This approach has been used to show the presence of (100) sites on cubic nanoparticles in an alkaline environment, and these particles showed activity comparable to Au(100) surfaces.[28] A similar structure sensitivity has been shown for Pt_3Ni nanoparticles in which Pt_3Ni octahedra have been shown to be more active than Pt_3Ni nanocubes, which is consistent with the predictions of our model.[30]

The constructed universal activity volcano shows a general trend of the left shift of the (100) volcano relative to the (111) volcano. As a result, we would expect the activity of metal nanoparticles that lie on the strong OH-binding leg of the volcano to be dominated by the (111) facet. As a result, we would expect the nanoparticle catalysts, on the strong binding leg of the volcano, to be less active than the (111) facet. This trend is seen in the much lower activity of the state-of-the-art nanoparticle Pt/C catalysts in comparison to the Pt(111) facet.[5] However, for materials whose (111) facet lies on the the weak OH-binding leg of the volcano, the corresponding (100) facet could lie on the strong binding leg of the volcano and still have an activity comparable to its (111) facet. This is a trend seen in the Pt_3Ni catalyst, where the (111) facet is active as a result of its favorable position on the right leg of the volcano, and the (100) facet is active as a result of its suitable position on the strong binding leg of the volcano. It is also experimentally shown that smaller Au nanoparticles[31] and larger Pt nanoparticles[32] have a higher specific activity for ORR, which is consistent with our model. Greeley et al.[3] also arrived at a similar conclusion for Au and Pt nanoparticles. We expect this to be a more general rule that the choice of nanoparticle catalysts should be such that the chosen metal has its dense facet on the weak binding leg of the volcano so that its more open facets and defects could also be active.

■ ASSOCIATED CONTENT

Supporting Information

The computational details and the computed binding energies of OH*, O* and OOH* on (111) and (100) surfaces are included. This material is available free of charge via the Internet at http://pubs.acs.org/.

■ AUTHOR INFORMATION

Corresponding Author

*E-mail: norskov@stanford.edu.

Notes

The authors declare no competing financial interest.

■ ACKNOWLEDGMENTS

The authors acknowledge support from the Department of Energy, Basic Energy Sciences through the SUNCAT Center for Interface Science and Catalysis. V.V. is grateful for a UTRC fellowship.

■ REFERENCES

(1) Nørskov, J. K.; Rossmeisl, J.; Logadottir, A.; Lindqvist, L.; Kitchin, J. R.; Bligaard, T.; Jonsson, H. *J. Phys. Chem. B* **2004**, *108*, 17886−17892.
(2) Greeley, J.; Stephens, I.; Bondarenko, A.; Johansson, T.; Hansen, H.; Jaramillo, T.; Rossmeisl, J.; Chorkendorff, I.; Nørskov, J. *Nat. Chem.* **2009**, *1*, 552−556.
(3) Greeley, J.; Rossmeisl, J.; Hellman, A.; Nørskov, J. K. *Z. Phys. Chem.* **2007**, *221*, 1209−1220.
(4) Karlberg, G. S.; Rossmeisl, J.; Nørskov, J. K. *Phys. Chem. Chem. Phys.* **2007**, *9*, 5158−5161.
(5) Stamenkovic, V. R.; Fowler, B.; Mun, B. S.; Wang, G.; Ross, P. N.; Lucas, C. A.; Markovic, N. M. *Science* **2007**, *315*, 493−497.
(6) Rossmeisl, J.; Karlberg, G. S.; Jaramillo, T.; Nørskov, J. K. *Faraday Discuss.* **2009**, *140*, 337−346.
(7) Man, I.; Su, H.; Calle-Vallejo, F.; Hansen, H.; Martínez, J.; Inoglu, N.; Kitchin, J.; Jaramillo, T.; Nørskov, J.; Rossmeisl, J. *ChemCatChem* **2011**, *3*, 1159−1165.
(8) Koper, M. T. M. *J. Electroanal. Chem.* **2011**, *660*, 254−260.
(9) Abild-Pedersen, F.; Greeley, J.; Studt, F.; Rossmeisl, J.; Munter, T. R.; Moses, P. G.; Skulason, E.; Bligaard, T.; Nørskov, J. K. *Phys. Rev. Lett.* **2007**, *99*, 016105.
(10) Stephens, I. E. L.; Bondarenko, A. S.; Perez-Alonso, F. J.; Calle-Vallejo, F.; Bech, L.; Johansson, T. P.; Jepsen, A. K.; Frydendal, R.; Knudsen, B. P.; Rossmeisl, J.; Chorkendorff, I. *J. Am. Chem. Soc.* **2011**, *133*, 5485−5491.
(11) Viswanathan, V.; Hansen, H.; Rossmeisl, J.; Jaramillo, T.; Pitsch, H.; Nørskov, J. K. *J. Phys. Chem. C* **2012**, *116*, 4698−4704.
(12) Wang, J. X.; Markovic, N. M.; Adzic, R. R. *J. Phys. Chem. B* **2004**, *108*, 4127−4133.
(13) Climent, V.; Gomez, R.; Orts, J. M.; Feliu, J. M. *J. Phys. Chem. B* **2006**, *110*, 11344−11351.
(14) Han, B. C.; Viswanathan, V.; Pitsch, H. *J. Phys. Chem. C* **2012**, *116*, 6174−6183.
(15) Kolb, D. *Prog. Surf. Sci.* **1996**, *51*, 109−173.
(16) Strmcnik, D. S.; Tripkovic, D. V.; van der Vliet, D.; Chang, K.-C.; Komanicky, V.; You, H.; Karapetrov, G.; Greeley, J.; Stamenkovic, V. R.; Marković, N. M. *J. Am. Chem. Soc.* **2008**, *130*, 15332−15339.
(17) Blizanac, B.; Lucas, C.; Gallagher, M.; Arenz, M.; Ross, P. N.; Marković, N. M. *J. Phys. Chem. B* **2004**, *108*, 625−634.
(18) Bondarenko, A. S.; Stephens, I. E. L.; Hansen, H. A.; Pérez-Alonso, F. J.; Tripkovic, V.; Johansson, T. P.; Rossmeisl, J.; Nørskov, J. K.; Chorkendorff, I. *Langmuir* **2011**, *27*, 2058−2066.
(19) Schmidt, T.; Stamenkovic, V.; Arenz, M.; Marković, N. M.; Ross, P. N. *Electrochim. Acta* **2002**, *47*, 3765−3776.
(20) Shao, M.; Huang, T.; Liu, P.; Zhang, J.; Sasaki, K.; Vukmirovic, M.; Adzic, R. R. *Langmuir* **2006**, *22*, 10409−10415.

(21) Blizanac, B.; Ross, P. N.; Marković, N. M. *J. Phys. Chem. B* **2006**, *110*, 4735−4741.
(22) Toda, T.; Igarashi, H.; Uchida, H.; Watanabe, M. *J. Electrochem. Soc.* **1999**, *146*, 3750−3756.
(23) Kleis, J.; Greeley, J.; Romero, N.; Morozov, V.; Falsig, H.; Larsen, A.; Lu, J.; Mortensen, J.; DuŁak, M.; Thygesen, K. *Catal. Lett.* **2011**, *141*, 1067−1071.
(24) Tritsaris, G.; Greeley, J.; Rossmeisl, J.; Nørskov, J. *Catal. Lett.* **2011**, *141*, 909−913.
(25) Ahmadi, T.; Wang, Z.; Green, T.; Henglein, A.; El-Sayed, M. *Science* **1996**, *272*, 1924−1926.
(26) Solla-Gullón, J.; Vidal-Iglesias, F.; Feliu, J. *Annu. Rep. Prog. Chem., Sect. C* **2011**, *107*, 263−297.
(27) Sanchez-Sanchez, C. M.; Solla-Gullon, J.; Vidal-Iglesias, F. J.; Aldaz, A.; Montiel, V.; Herrero, E. *J. Am. Chem. Soc.* **2010**, *132*, 5622−5624.
(28) Hernandez, J.; Solla-Gullon, J.; Herrero, E.; Aldaz, A.; Feliu, J. M. *J. Phys. Chem. C* **2007**, *111*, 14078−14083.
(29) Sanchez-Sanchez, C. M.; Vidal-Iglesias, F. J.; Solla-Gullón, J.; Montiel, V.; Aldaz, A.; Feliu, J. M.; Herrero, E. *Electrochim. Acta* **2010**, *55*, 8252−8257.
(30) Zhang, J.; Yang, H.; Fang, J.; Zou, S. *Nano Lett.* **2010**, *10*, 638−644.
(31) Tang, W.; Lin, H.; Kleiman-Shwarsctein, A.; Stucky, G. D.; McFarland, E. W. *J. Phys. Chem. C* **2008**, *112*, 10515−10519.
(32) Shao, M.; Peles, A.; Shoemaker, K. *Nano Lett.* **2011**, *11*, 3714−3719.